Journal of Electronic Materials (2024) 53:2351–2366
https://doi.org/10.1007/s11664-024-11000-4

ORIGINAL RESEARCH ARTICLE

Effect of Oxygen Flow Rate, Post-annealing Temperature, and Different Electrolyte Concentrations on WO_3 Thin Films Deposited by DC Magnetron Sputtering For Electrochromic Applications

K. Naveen Kumar[1,2] · G. V. Ashok Reddy[1] · Sheik Abdul Sattar[1] · R. Imran Jafri[3] · R. Premkumar[4] · M. Muthukrishnan[5] · A. Asrar Ahamed[6] · M. R. Meera[7] · Nunna Guru Prakash[8] · Ammar M. Tighezza[9] · Tae Jo Ko[8]

Received: 8 August 2023 / Accepted: 22 February 2024 / Published online: 18 March 2024

Abstract

In this work, tungsten oxide (WO_3) films were deposited at room temperature and annealed for 2 h at 400°C. The electrochromic and electrochemical properties were studied for two different electrolytes. The films were deposited at different oxygen flow rates of 2, 4, and 6 standard cubic centimeters per minute (SCCM). X-ray diffraction analysis revealed structural characterization of amorphous and crystalline phases. UV-visible spectroscopy optical transmittance revealed 91% transmittance, and energy-dispersive x-ray spectroscopy (EDS) analysis revealed the absence of impurities and the presence of W and O. An electrochemical analyzer was used to characterize the deposited and annealed WO_3 films immersed in the two different electrolyte solutions (H_2SO_4 and $LiClO_4$ with oxygen flow rates ranging from 2 SCCM to 6 SCCM). It was found that the H_2SO_4 electrolyte of an annealed WO_3 thin film at 2 SCCM demonstrated high coloring efficiency of 50.18 cm^2/C, and the $LiClO_4$ electrolyte of an annealed WO_3 thin film at 4 SCCM demonstrated high coloring efficiency of 20.06 cm^2/C.

Keywords Oxygen flow rates · electrochromic properties · sputtering · H_2SO_4 · $LiClO_4$ electrolytes

Introduction

With the continuing rapid depletion of fossil fuel materials, renewable energy sources are increasingly used for electrochemical capacitors.[1,2] Up to 30–40% of the primary energy consumed worldwide is utilized for heating, cooling, ventilation, and electrical appliances in buildings.[3–5] Therefore, the use of materials in buildings that can convert and store energy from renewable sources is beneficial. By applying a small electric field, electrochromic substances can change their optical characteristics such as transmittance, reflection, and absorption in a reversible manner. This property makes them extremely appealing for a variety of potential

✉ K. Naveen Kumar
naveenkilari95@gmail.com

✉ Sheik Abdul Sattar
sheik.abdul.sattar@nmit.ac.in

✉ Nunna Guru Prakash
drguruprakashn@gmail.com

✉ Tae Jo Ko
tjko@yu.ac.kr

[1] Department of Physics, Nitte Meenakshi Institute of Technology, Yelahanka, Bengaluru 560064, India

[2] Centre for Nano-materials and MEMS, Nitte Meenakshi Institute of Technology, Yelahanka, Bengaluru 560064, India

[3] Department of Physics and Electronics, Christ University, Hosur Road, Bengaluru 560029, India

[4] Department of Physics, N.M.S.S.V.N. College, Nagamalai, Madurai, Tamil Nadu 625019, India

[5] Department of Physics, Sona College of Technology, Salem, Tamil Nadu 636005, India

[6] Department of Chemistry, Jamal Mohamed College (Autonomous), Affiliated to Bharathidasan University, Trichy, Tamil Nadu 620020, India

[7] Department of Physics, Sree Ayyappa College for Women, Chunkankadai, Nagercoil, Tamil Nadu 629 003, India

[8] School of Mechanical Engineering, Yeungnam University, 280 Daehak-ro, Gyoungsan-si, Gyeongsangbuk-do 38541, Republic of Korea

[9] Department of Chemistry, College of Science, King Saud University, P. O. Box 2455, 11451 Riyadh, Saudi Arabia

applications, including large-area information displays, antiglare automobile mirrors, and energy-efficient smart windows.[6,7]

Numerous studies have been conducted on tungsten trioxide (WO_3), which has been named one of the most interesting inorganic electrochromic compounds.[8,9] An electrochromic material should have 100% optical modulation, meaning that it should be totally opaque while colored and fully transparent when bleached. The coloration efficiency (CE) and kinetics will depend on the morphological, structural, and compositional characteristics, and the suitability for use in a variety of devices, including solar cells,[10,11] smart windows,[12–15] gas sensors,[16] and photodetectors.[17] The electrochemical equation below[18] controls the electrochromism reaction in WO_3:

$$WO_3(\text{colorless}) + xM^+ + xe^- \leftrightarrow MxWO_3(\text{dark blue}) \quad (1)$$

where x is the ion concentration, and M represents K^+, H^+, Na^+, or Li^+ ions. Various deposition techniques have been used for WO_3 films including sol–gel,[19] hot-filament-assisted synthesis,[20] sputtering,[21–33] electron beam evaporation,[34,35] electrodeposition processing,[36] and hydrothermal[37–41] and solvothermal techniques.[42] Overall, relatively little research on sputtering-fabricated WO_3 films has been published. Furthermore, up to this point, we were unable to locate any other research in the literature demonstrating the influence of the deposition oxygen flow rate (OFR) on the electrochromic properties of WO_3 films produced by sputtering. Therefore, we present a thorough investigation of the effects of various oxygen flow deposition rates, post-annealed WO_3 films, and various electrolyte solutions on the optical, structural, electrochromic, and electrochemical attributes of WO_3 films deposited by the sputtering technique in the current work. Here, we discuss how various OFRs affect the structural, optical, and electrochromic characteristics of sputtering. WO_3 films were produced, and efforts were made to optimize the OFR, the electrolyte solution, and the nature of the film (amorphous or crystalline) for use in electrochromic applications.

Experimental Techniques

Method to Produce Thin Films of WO_3

A popular physical vapor deposition (PVD) technique known as direct current (DC) magnetron sputtering was used to deposit the WO_3 films on Corning glass and fluorine-doped tin oxide (FTO) substrates. Before being fed into the sputtering chamber, the glass samples were cleaned with a soap solution and deionized water (DI) using ultrasonication. The tungsten metal disc was used as the sputter target and it was sputtered in an atmosphere of argon (Ar) and oxygen (O_2). The base vacuum of the sputtering chamber was maintained at 2×10^{-6} mbar. In order to remove impurities that had been adsorbed onto the target surface pre-sputter, the tungsten target was subjected to an argon gas atmosphere for 10 min. The WO_3 films were produced under OFRs of 2, 4, and 6 standard cubic centimeters per minute (SCCM) at room temperature (RT). A constant 100 mA DC current was used during the whole deposition.

Characterization

X-ray diffraction (XRD; Rigaku MiniFlex, Rigaku Corporation) was used to analyze the crystallization of the films. Raman spectroscopy (Renishaw plc) was used to analyze the chemical bonding. The optical absorption behavior was characterized using an ultraviolet–visible spectrometer (SPECORD S600). An electrochemical workstation (SP-300 BioLogic) was used for all electrochemical analyses. The workstation has a three-electrode setup with a platinum wire as the counter electrode (CE), $Hg_2/HgCl_2$ as the reference electrode (RE), and WO_3 thin film as the working electrode (WE). An aqueous solution of 0.5 M H_2SO_4 and a non-aqueous solution of 0.5 M $LiClO_4$ were used as electrolytes, and the sweep voltage was maintained between −0.7 and +1 V at scan rates of 20 mV/s.

Results and Discussion

XRD Analysis

Figure 1a displays the XRD characteristics of the WO_3 films that were deposited using DC sputtering at various OFRs. The RT-deposited samples exhibit amorphous characteristics at various OFRs, according to the XRD evaluation. Amorphous films are produced on a glass substrate that has not been heated when different amounts of PaO_2 are deposited using DC and RF sputtering, according to studies by Madhavi et al.[43] and Mohamed et al.[44]

An eventual change in film crystallinity is the most fundamental effect of the annealing process. Consequently, XRD analysis was used to characterize the WO_3 films annealed at 400°C for 2 h in order to investigate the change in the crystal structure. The XRD patterns of heat-treated WO_3 films after 2 h at 400°C are clearly shown in Fig. 1b, which reveals the presence of distinctive diffraction peaks corresponding to the WO_3 planes. For different oxygen partial pressures, the XRD spectra that are produced show that the 400°C air-annealed sample is crystalline.[25] DC-sputtered WO_3 films have 2θ values of 14.04°, 23.38°, 24.47°, 28.16°, 33.89°, 36.93°, 50.09°, and 56.09°, and their hkl values are (100), (002),

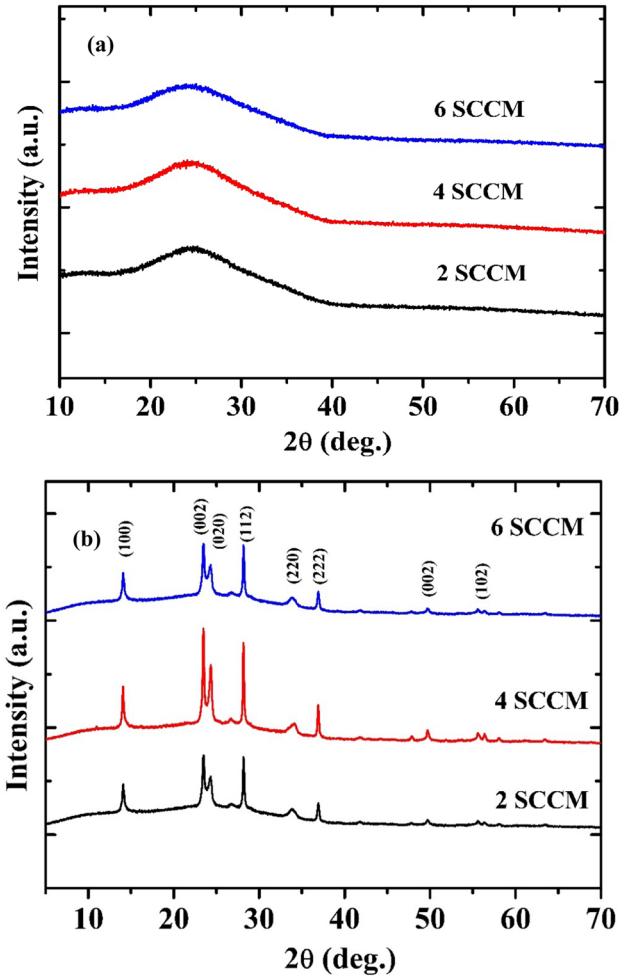

Fig. 1 XRD spectra of WO_3 films deposited at various OFR: (a) RT and (b) annealed.

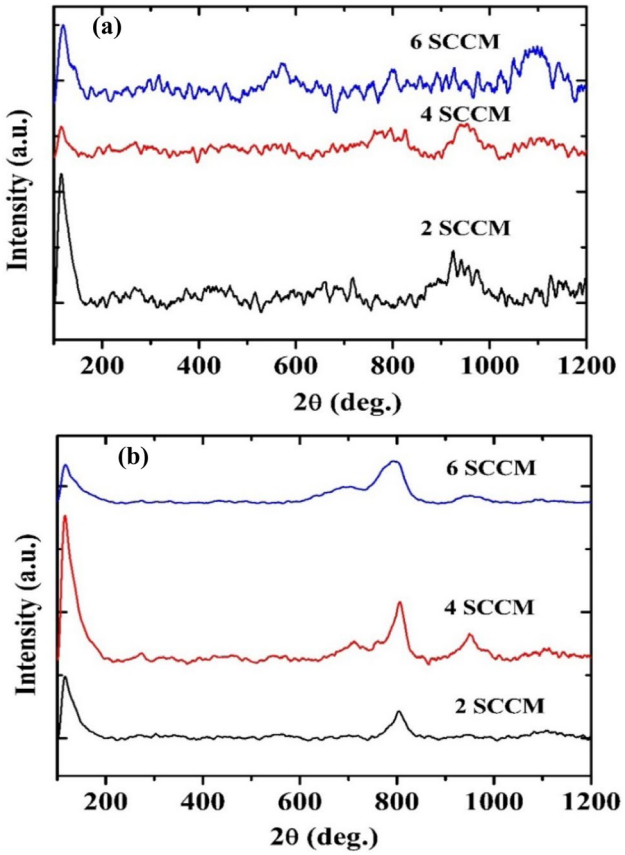

Fig. 2 Raman spectra of WO_3 films at various OFRs: (a) RT and (b) annealed.

(020), (112), (220), (222), (002), and (102), respectively. There were differences in OFRs between 2 and 6 SCCM. For increased OFRs, WO_3 films have a crystalline character, due to the annealing at 400°C.

Raman Analysis

The Raman spectra of the WO_3 films at various OFRs are shown in Fig. 2a and b. Because of the W–O bonds, the spectra of the as-deposited film exhibit a significant peak at 770 cm^{-1}, as shown in Fig. 3a.[45] The appearance of this peak corresponds with the two strongest peaks at 719 and 807 cm^{-1} in the Raman spectrum of the crystalline WO_3 films. The W=O stretching mode of terminal oxygen atoms is attributed to a rather steep peak at 950 cm^{-1}, which may occur on the surfaces of the cluster and microvoid structures in the film.[9] A weaker, broad peak is also present at 220 cm^{-1}, which is attributed to the presence of W^{4+} states. Figure 2b displays the Raman spectra that were recorded for the WO_3 annealed films. The spectra of WO_3 films annealed at 400°C for 2 h at various OFRs exhibit a broad peak in the range of 100–1200 cm^{-1} due to the O–W–O stretching vibration mode, which denotes the growth of sub-stoichiometric WO_3 films of mixed metallic tungsten and tungsten oxide. Sharp Raman peaks, representing the bending and stretching vibration modes of the O–W–O bond, can be seen at 695 and 809 cm^{-1}[46] when the OFR increases from 2 to 6 SCCM.

Optical Properties

Figure 3 illustrates the transmittance plots of WO_3 films for both RT and post-annealing at 400°C for 2 h at different OFRs. The transmittance is increased with respect to the increase in OFR for RT-deposited samples, and transmittance is decreased for annealed samples.[47,48] The transmittance is more than 82% at a wavelength of 700 nm for RT samples at different OFRs, and transmittance is less for the sample annealed at 4 SCCM. The transmittance values for annealed and RT samples are shown in Table I.

Electrochemical Properties

The electrochemical properties determine the structure of the electrochromic WO_3 thin film, which is employed as the working electrode. Hg/HgCl serves as the reference electrode, and a Pt needle serves as the counter electrode. For the half cell, 0.5 M H_2SO_4 and $LiClO_4$ solution were prepared as electrolytes. The cyclic voltammetry (CV) curves of WO_3 films were recorded in the potential range of −0.7 to 1 V at a scan rate of 20 mV s^{-1}. When a negative voltage is supplied to the working electrode, the color changes from transparent to blue. When a positive voltage is applied, the film becomes transparent.[49]

Figures 4a and b and 6a and b show typical broad featureless peaks in the CV characteristics that represent the insertion and extraction of H^+ and Li^+ ions into WO_3 films. The cathodic peak current of WO_3 films at RT in the H_2SO_4 electrolyte solution, as measured by the CV curves (measured at −0.7 V), initially decreased from −2.98 mA/cm^2 at 2

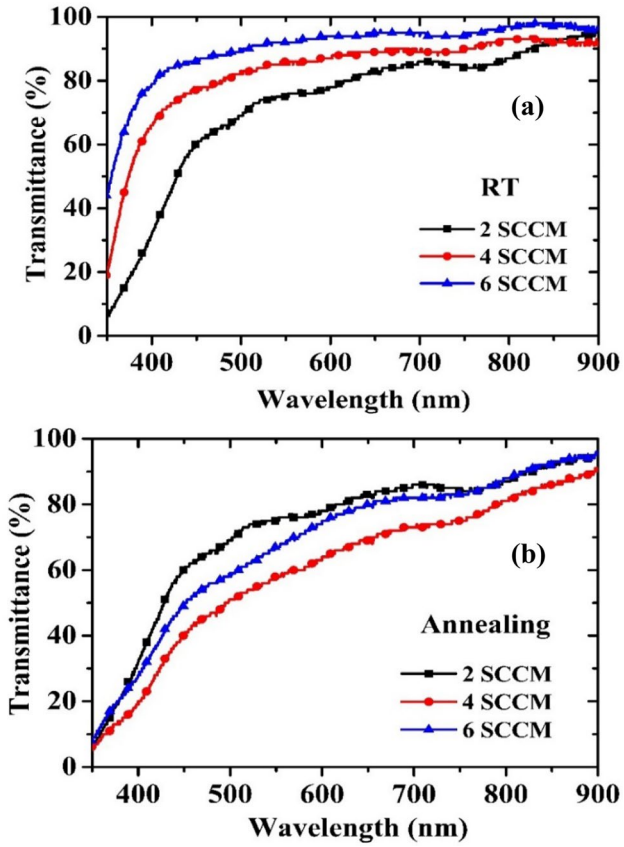

Fig. 3 Transmittance plots of WO_3 films deposited at various OFRs: (a) RT and (b) annealed.

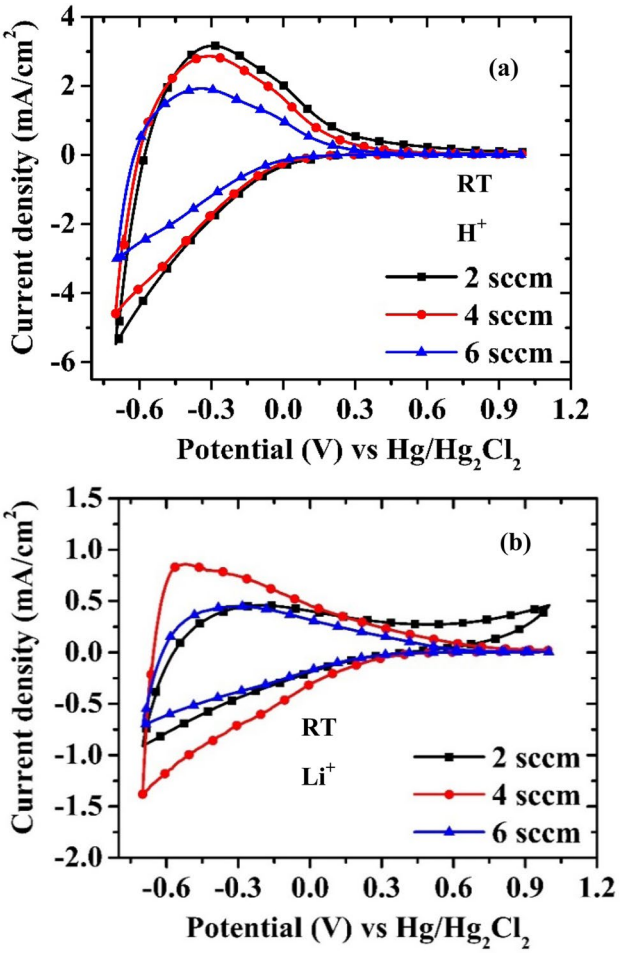

Fig. 4 Cyclic voltammograms of WO_3 films deposited at RT for various OFRs: (a) 0.5 M H_2SO_4 (H^+) and (b) 0.5 M $LiClO_4$ (Li^+).

Table I Comparison of transmittance of WO_3 films before annealing and after annealing at various OFRs

WO_3 film	Oxygen flow rate (SCCM)	Transmittance (%) at 500 nm	Transmittance (%) at 600 nm	Transmittance (%) at 700 nm
RT	2	69	78	86
	4	83	87	89
	6	90	94	95
Annealing at 400 °C	2	69	78	86
	4	51	63	73
	6	58	74	82

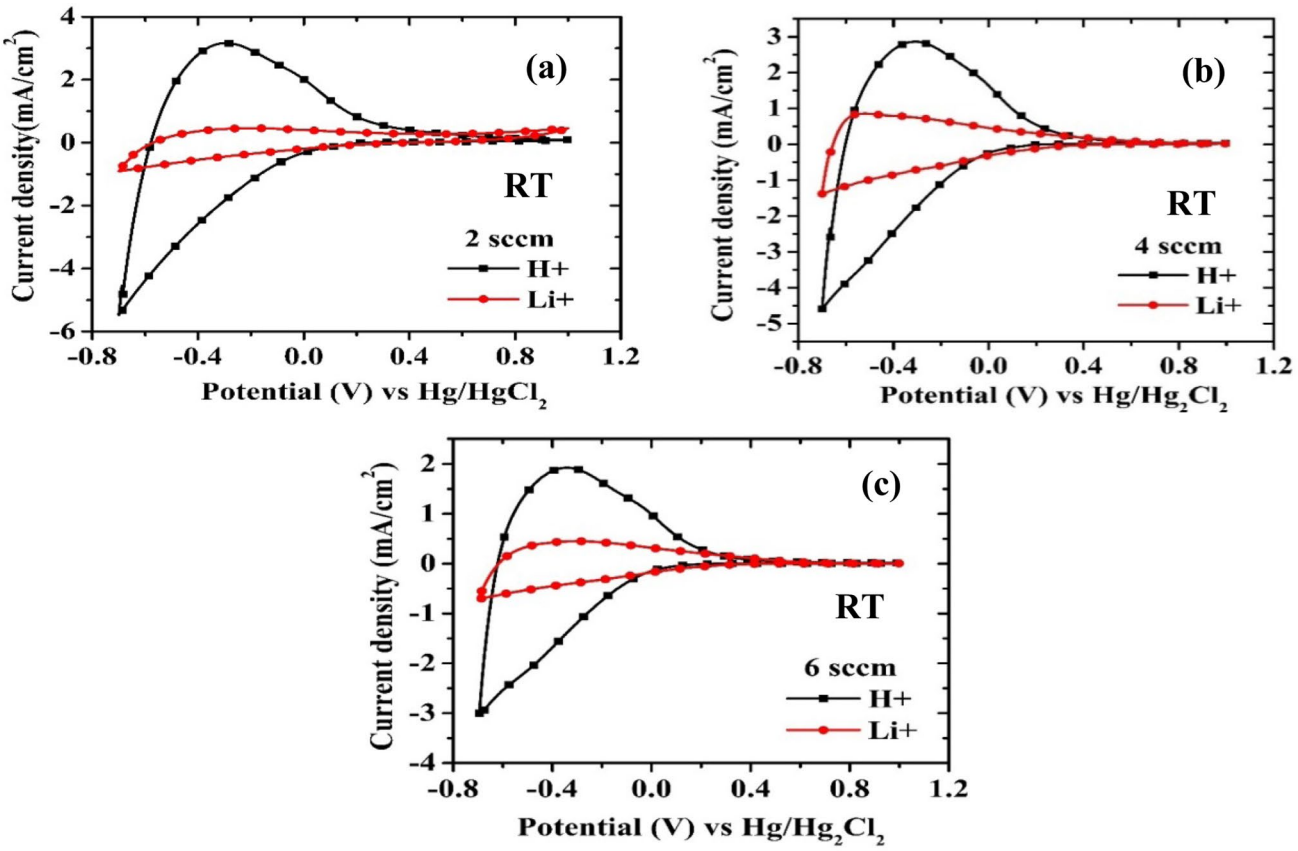

Fig. 5 Comparison plots of CV curves of WO_3 films deposited at RT at various OFRs: (a) 2 SCCM, (b) 4 SCCM, and (c) 6 SCCM.

SCCM to −5.40 mA/cm^2 at 6 SCCM OFR. This increase in OFRs eventually led to an increase in cathodic peak current as shown in Fig. 4a. The cathodic peak current of WO_3 films at RT in $LiClO_4$ electrolyte solution is shown in Fig. 4b. The CV curves initially decreased from −0.83 mA/cm^2 at 2 SCCM to −1.42 mA/cm^2 at 4 SCCM. This increase in OFRs ultimately led to an increase in cathodic peak current back to −0.74 mA/cm^2 at 6 SCCM OFRs (Fig. 5). Figure 6 shows the first and 50th cyclic voltammetry curves of WO_3 film deposited at RT, which reveal that the performance of the thin film was severely degraded and the stability decreased after 50 cycles. The reversibility decreased slightly as the number of cycles increased. The film contained certain irreversible deep trap sites, which prevented the electrochromic reversibility from reaching 100%. The area of the voltammogram decreased with an increase in the electrochemical cycle. An increase in voltage was observed with a decrease in current. The charge insertion capability of the film also decreased with increased cycles.[50] The cathodic peak current of WO_3 films in the H_2SO_4 electrolyte solution that was annealed at 400°C for 2 h showed a CV curve that initially decreased from −0.74 mA/cm^2 at 2 SCCM to −0.92 mA/cm^2 at 4 SCCM, as shown in Fig. 7a. However, as OFRs increased, the cathodic peak current eventually increased back to −0.87 mA/cm^2 at 6 SCCM OFRs. The lowest cathodic peak current of all the CV curves is shown in Fig. 7b, which represents the cathodic peak current of annealed at 400°C in 2 h of WO_3 films in $LiClO_4$ electrolyte solution. The CV curves are recorded as −0.55 mA/cm^2 at 2 SCCM, −0.48 mA/cm^2 at 4 SCCM, and −0.39 mA/cm^2 at 6 SCCM OFRs. Figures 5 and 8 show the comparison plots of CV curves of WO_3 films RT and annealed for OFRs of 2 SCCM, 4 SCCM, and 6 SCCM. The Randles–Ševčík equation can be used to calculate the diffusion coefficient, D, for the H^+ and Li^+ ions.[51]

$$D^{1}/2 = \frac{i_{\mathrm{P}}}{C_o \times A \times 10^5 \times 2.69 \times n^{3}/2 \times \nu^{1}/2} \tag{2}$$

where i_p, n, A, C_o, v, and D are peak current, number of electrons, area of the active WO_3 film, electrolyte concentration, scan rate, and diffusion coefficient, respectively.

Table II summarizes the determined diffusion coefficients of the WO_3 films and annealed 400°C in 2 h of the WO_3 films in both H_2SO_4 and $LiClO_4$ electrolyte solutions treated at increasing OFRs. It is obvious that the diffusion coefficient (DC) is influenced by the OFRs and different electrolytes. Amorphous WO_3 films in H_2SO_4 electrolyte treated

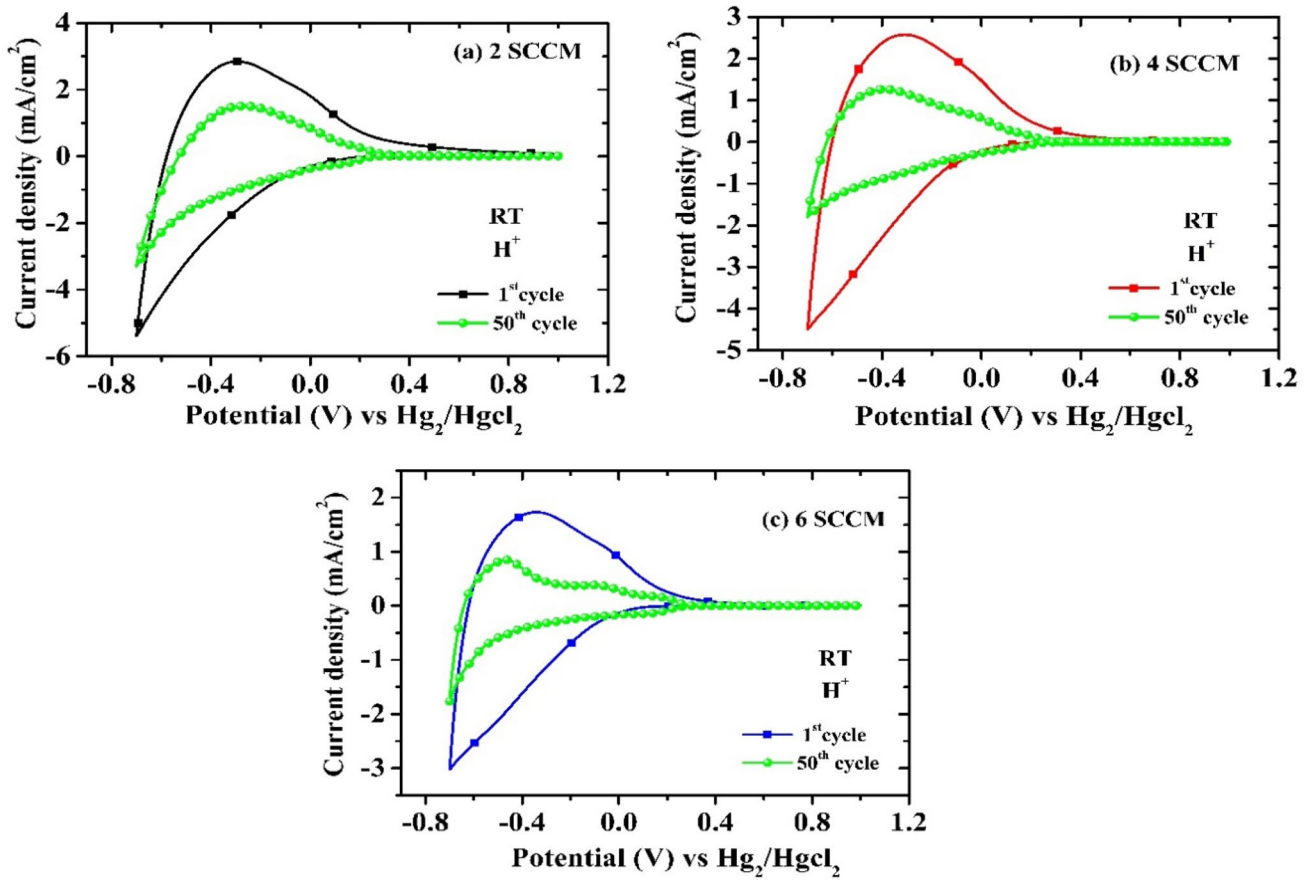

Fig. 6 CV plots of WO_3 thin films: (a) 2 SCCM, (b) 4 SCCM, and (c) 6 SCCM after 50 cycles in H_2SO_4 electrolyte solution at RT.

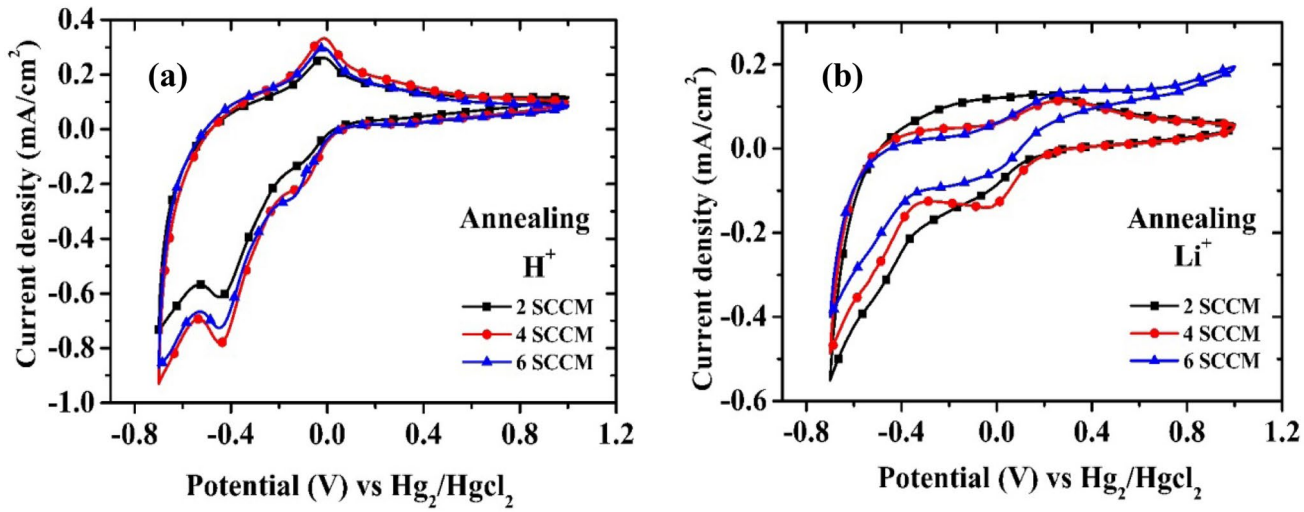

Fig. 7 Cyclic voltammograms of WO_3 films annealed at 400°C for various OFRs: (a) 0.5 M H_2SO_4 (H^+) and (b) 0.5 M $LiClO_4$ (Li^+).

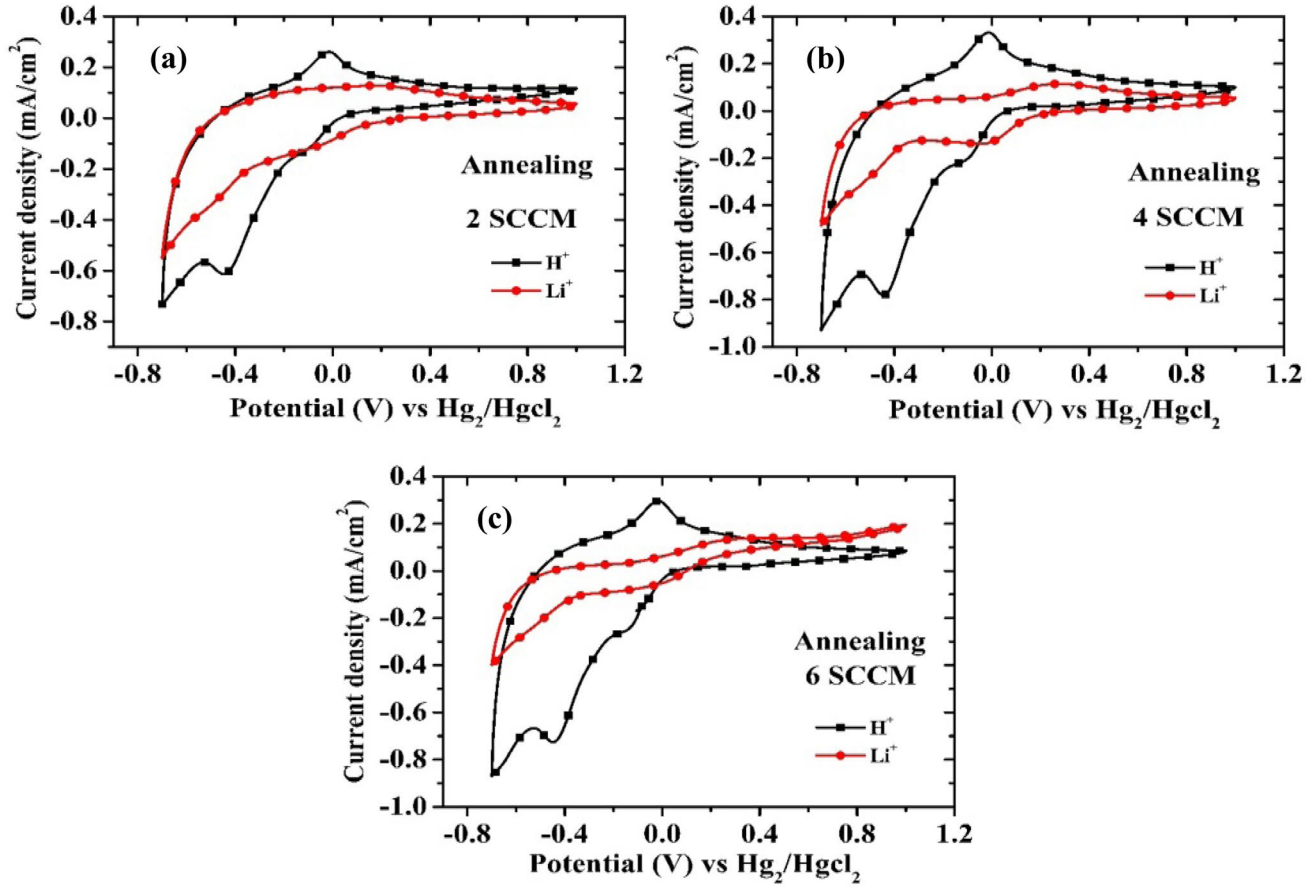

Fig. 8 Comparison plots of CV curves of WO_3 films annealed at 400°C for various OFRs: (a) 2 SCCM, (b) 4 SCCM, and (c) 6 SCCM.

Table II Diffusion coefficients of comparison for before annealing and after annealing WO_3 films in H_2SO_4 (H^+) and $LiClO_4$ (Li^+) electrolytes and various OFRs

Name of electrolyte	WO_3 films	Oxygen flow rate (SCCM)	Cathodic peak current i_p (mA)	Diffusion coefficient D (cm^2/s)
H_2SO_4 (H^+)	RT	2	−2.98	1.007×10^{-7}
		4	−4.60	7.05×10^{-8}
		6	−5.40	3.17×10^{-8}
	Annealed	2	−0.749	1.468×10^{-9}
		4	−0.929	2.323×10^{-9}
		6	−0.870	2.102×10^{-9}
$LiClO_4$ (Li^+)	RT	2	−0.83	2.16×10^{-9}
		4	−1.42	6.02×10^{-9}
		6	−0.74	1.59×10^{-9}
	Annealed	2	−0.550	8.50×10^{-10}
		4	−0.485	6.689×10^{-10}
		6	−0.399	4.538×10^{-10}

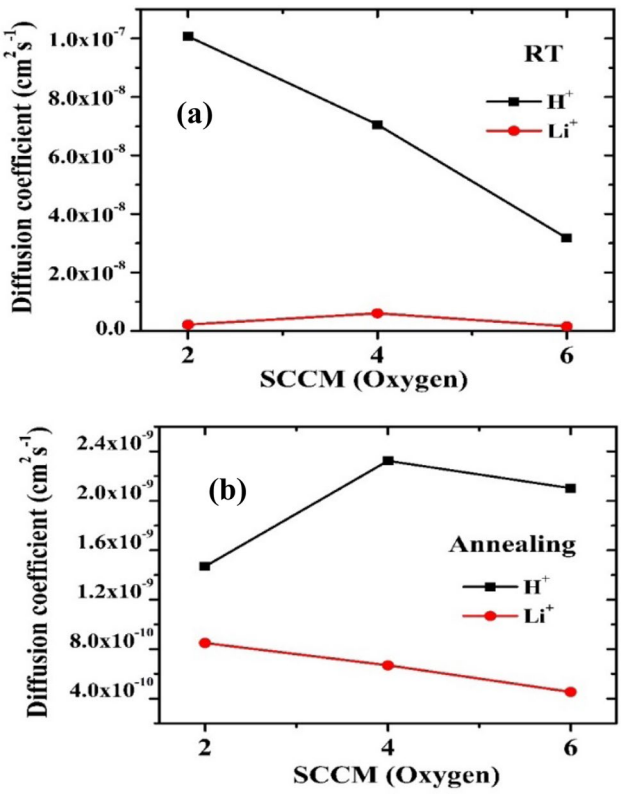

Fig. 9 Diffusion coefficients comparison plots of (a) RT and (b) annealed WO_3 films at H_2SO_4 (H^+) and $LiClO_4$ (Li^+) electrolytes and various OFRs.

at 2 SCCM OFR demonstrated a maximum diffusivity of 1.007×10^{-7} cm^2/s, which is two orders of magnitude higher than the 1.59×10^{-9} cm^2/s of the amorphous WO_3 films in $LiClO_4$electrolyte at 6 SCCM OFR. Additionally, crystalline WO_3 films in H_2SO_4 electrolyte treated at 4 SCCM OFR showed the highest diffusivity of 2.32×10^{-9} cm^2/s, which is an order of magnitude higher than the 4.53×10^{-10} cm^2/s of the crystalline WO_3 films in $LiClO_4$ electrolyte at 6 SCCM OFR. These films were post-annealed at 400°C for 2 h. Finally, amorphous WO_3 films in an electrolyte of H_2SO_4 at a 2 SCCM OFR revealed the highest DC of 1.007×10^{-7} cm^2/s in comparison to crystalline WO_3 films in an electrolyte of $LiClO_4$ at 6 SCCM OFR, as shown in Fig. 9. Similar findings were reported by Madhavi et al., who found that the blockage of insertion sites was the reason for the decrease in DC at higher annealing temperatures.[52] Hsu et al. explained that although there is a driving force from the applied voltage, the compact film structure prevented Li^+ ions from intercalating in MoO_3 electrochromic films that were produced using a sol–gel technique, which reduced the DC.[53]

Electrochromic Studies

Figures 10 and 11 show the optical transmission spectra of the WO_3 films in their corresponding colored and bleaching states in the 300–900 nm range. The optical transmittance spectra of the DC-sputtered WO_3 films were investigated by UV-visible spectroscopy. Figure 10a, b, c, d, and e displays the transmittance for the bleached and colored states obtained for various OFRs (2 SCCM, 4 SCCM, and 6 SCCM) and two different electrolyte solutions (H_2SO_4 and $LiClO_4$). As shown in Fig. 11a, b, and c, the observed values of transmittance at a wavelength of 600 nm range from 0% for 2 SCCM, 1% for 4 SCCM, 5% for 6 SCCM for the colored state, and 58% for 2 SCCM, 85% for 2 SCCM, and 91% for 6 SCCM for the bleached state of WO_3 films in 0.5 M H_2SO_4 electrolyte solution. In the colored state of the WO_3 films in the 0.5 M $LiClO_4$ electrolyte solution, the observed values of transmittance at a wavelength of 600 nm range from 19% for 2 SCCM, 10% for 4 SCCM, and 22% for 6 SCCM; and in the bleached state, the values are 43% for 2 SCCM, 81% for 2 SCCM, and 90% for 6 SCCM, as shown in Fig. 10d and e. Also, as measured for different OFRs (2 SCCM, 4 SCCM, and 6 SCCM) and two different electrolyte solutions (H_2SO_4 and $LiClO_4$), the transmittance of annealed WO_3 films (crystalline) for bleached and colored states is shown in Fig. 11 a, b, c, d, and e. As shown in Fig. 11a, b, and c, the observed values of transmittance at a wavelength of 600 nm range from 9% for 2 SCCM, 8% for 4 SCCM, and 15% for 6 SCCM for the colored state, and 66% for 6 SCCM for the bleached state of crystalline WO_3 films in 0.5 M H_2SO_4 electrolyte solution. Figure 11d, e, and f shows the observed values of transmittance at a wavelength of 600 nm for crystalline WO_3 films in 0.5 M $LiClO_4$ electrolyte solution. The observed values range from 42% for 2 SCCM, 41% for 4 SCCM, and 64% for 6 SCCM for the colored state, and 68% for 2 SCCM, 60% for 2 SCCM, and 70% for 6 SCCM bleached state. We may deduce from this result that if OFRs in both electrolytes are increased, the films become less intensely colored because fewer ions are available for intercalation, making them less opaque and increasing the transmittance for the colored state.

The transmittance of these transition metal oxides in both transparent and opaque phases, which is necessary for electrochromic applications, is one of their most important properties. As a result, there is a significant optical modulation, or ΔOT, which is measured as the difference between the transmittance of the colored and bleached states.[54] The host matrix's trapped ions play a part in the material's

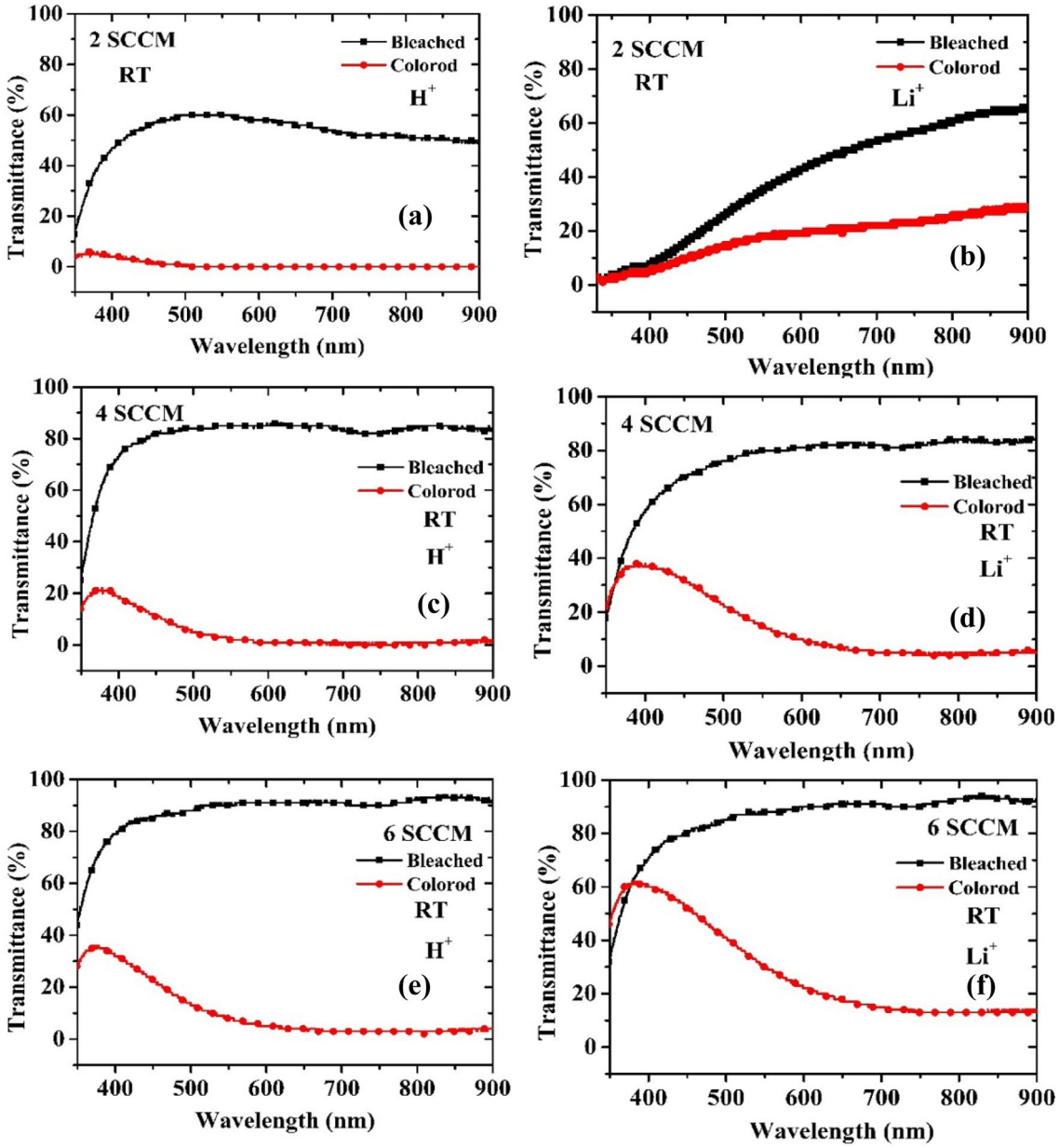

Fig. 10 Transmittance plots of colored and bleached states of RT WO_3 films: (a) 2 SCCM, (c) 4 SCCM, and (e) 6 SCCM for H_2SO_4 (H^+) solution and (b) 2 SCCM, (d) 4 SCCM, and (f) 6 SCCM for $LiClO_4$ (Li^+) solution.

degraded electrochromic performance. Because the intercalated H^+ ions are not entirely removed from the formed film, degradation in optical modulation of the host matrix can be detected during specific voltage cycles. CV measurements were performed, and the bleached and colored switching characteristics of WO_3 and post-annealed WO_3 films in H_2SO_4 and $LiClO_4$ in two different electrolyte solutions of 0.5 M concentration were recorded at a scan rate of 10 mV/s and applied potential of −0.7 to 1 V. The results are shown in Table III for the various OFRs, as well as the WO_3 and post-annealed WO_3 films. The optical modulation of amorphous WO_3 films in H_2SO_4 electrolyte solution is greatest at 6 SCCM OFR. However, WO_3 films that were annealed at 400°C displayed very low bleaching and

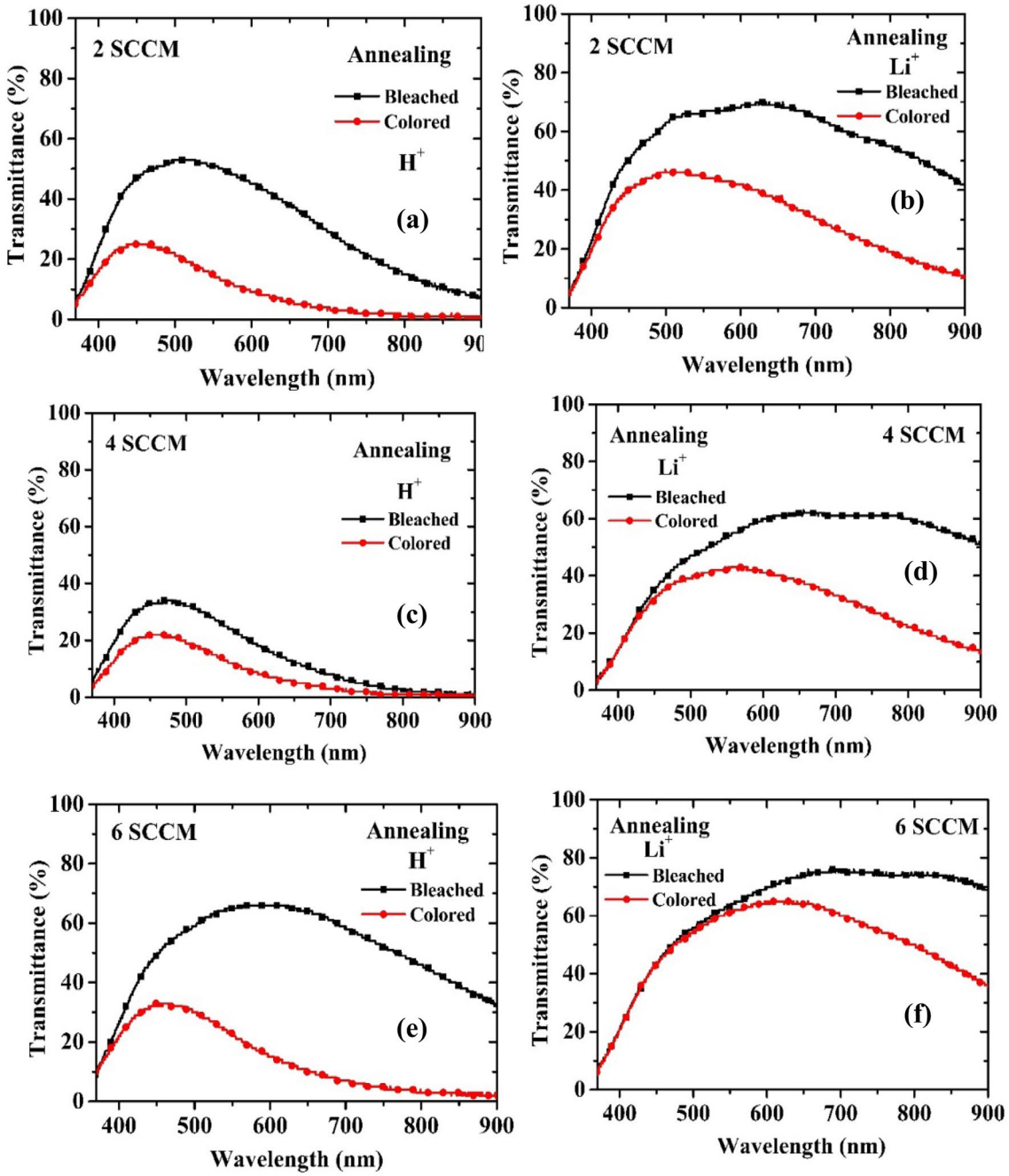

Fig. 11 Transmittance plots of colored and bleached states of annealed WO_3 films: (a) 2 SCCM, (c) 4 SCCM, and (e) 6 SCCM for H_2SO_4 (H^+) solution and (b) 2 SCCM, (d) 4 SCCM, and (f) 6 SCCM for $LiClO_4$ (Li^+) solution.

coloring transmittances, which is indicative of weak electrochromic characteristics. The crystalline WO_3 films in $LiClO_4$ electrolyte were unable to recover to their initial transparent form despite having poor transmittance in the colored state. Figure 12a and b shows the bleached and colored states obtained during oxidation and reduction, respectively. The coloring and bleaching times of the electrochromic films are plotted using chronoamperometry in Fig. 10. We fixed the pulse interval to 10 s, the start voltage to −0.7 V, and the upper limit voltage to 1 V for the chronoamperometry (CA) curve experiment using H_2SO_4 as the electrolyte. The response period for oxidation and reduction is the amount of time required for the anodic and cathodic currents to equalize when voltages are applied. The coloration time for 2 SCCM, 4 SCCM, and 6 SCCM of WO_3 samples is 3.2, 3.7, and 3.3 s, respectively, and the bleach time for 2 SCCM, 4

Table III Comparison of optical modulation, coloration efficiency, bleaching, and coloration transmittance before annealing, after annealing WO_3 films in H_2SO_4 (H^+) and $LiClO_4$ (Li^+) electrolytes at various OFRs

Electrolyte	WO_3 films	Oxygen flow rate (SCCM)	Transmittance (%)		Optical modulation ($\Delta T = T_b - T_c$%)	CE (cm^2/C)
			Bleaching (T_b)	Coloring (Tc)		
H_2SO_4 (H^+)	RT	2	58	0	58	22
		4	85	1	84	21.16
		6	91	5	86	20.54
	Annealed	2	45	9	36	50.18
		4	18	8	10	16.64
		6	66	15	51	33.75
$LiClO_4$ (Li^+)	RT	2	43	19	24	19.10
		4	81	10	71	27.44
		6	90	22	68	18.46
	Annealed	2	68	42	26	20.06
		4	60	41	19	18.25
		6	70	64	6	4.92

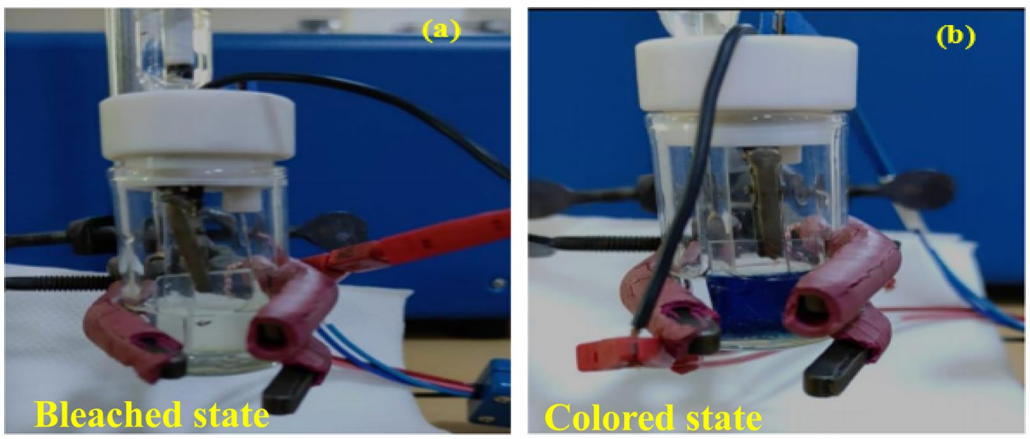

Fig. 12 (a) Bleached and (b) colored states of WO_3 thin film.

SCCM, and 6 SCCM of WO_3 samples is 1.7, 2.8, and 1.3 s, respectively. The outcome demonstrates that all deposited films took longer to color than to bleach (Fig. 13).

The ratio of the change in optical density to the incorporated charge per unit area is known as the coloring efficiency (CE), and it is one of the most important parameters for assessing the effectiveness of electrochromic products. It can be calculated using the formula shown below[55]:

$$\mathrm{CE} = \Delta\mathrm{OD} \Big/ \frac{Q}{A} \tag{3}$$

$$\Delta\mathrm{OD} = \mathrm{Log}\frac{T_b}{T_c} \tag{4}$$

where T_b is the bleached transmittance, T_c is the color transmittance, Q_{in} is the incorporated charge, and ΔOD is the optical density. Using T_b and T_c from Table III, the CE of the WO_3 films at 600 nm was then calculated as follows. For different OFRs, the calculated CE of the WO_3 films (amorphous) was found to be 22 cm^2/C at 2 SCCM, 21.16 cm^2/C at 4 SCCM, 20.54 cm^2/C at 6 SCCM in H_2SO_4 electrolyte solution, and 19.10 cm^2/C at 2 SCCM, 27.44 cm^2/C at 4 SCCM, and 18.46 cm^2/C at 6 SCCM in $LiClO_4$ electrolyte solution, respectively. The calculated CE of the heated WO_3 films (crystalline) at 400°C for 2 h was found to be 50.18 cm^2/C at 2 SCCM, 16.64 cm^2/C at 4 SCCM, and 33.75 cm^2/C at 6 SCCM in H_2SO_4 electrolyte solution, and 20.06 cm^2/C at 2 SCCM, 18.25 cm^2/C at 4SCCM, and 4.92 cm^2/C at 6 SCCM in $LiClO_4$ electrolyte solution, respectively. According to CE results, crystalline WO_3 films in an electrolyte concentration of H_2SO_4 performed better in an electrochemical cell than amorphous WO_3 films in an electrolyte concentration of $LiClO_4$, as shown in Fig. 14.

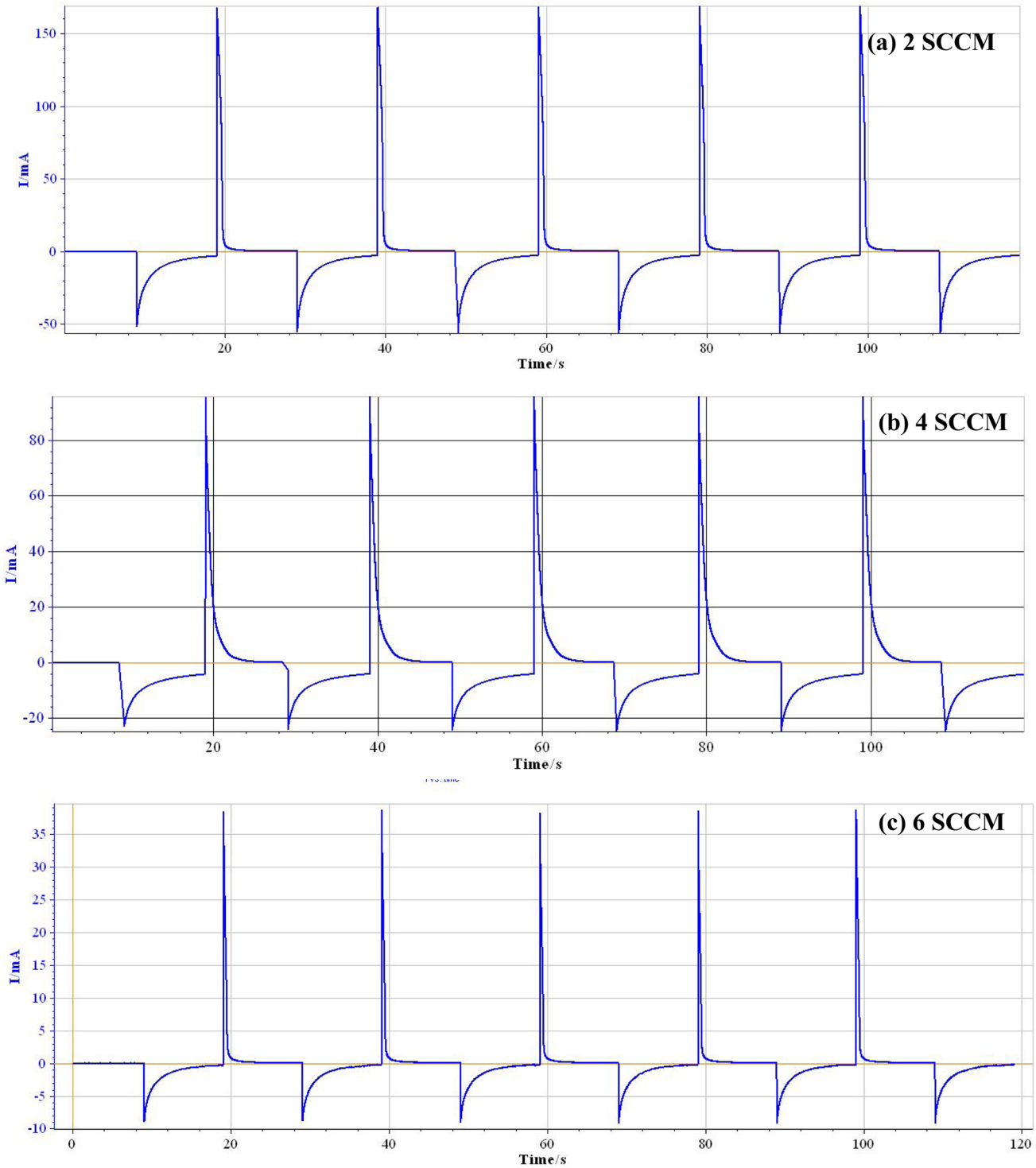

Fig. 13 CA plots of WO_3 thin films: (a) 2 SCCM, (b) 4 SCCM, and (c) 6 SCCM after 50 cycles in H_2SO_4 electrolyte solution at RT.

In this study, we propose the coexistence of amorphous and crystalline phases in WO_3 films annealed at 400°C at various OFRs (2, 4, and 6 SCCM) in two different electrolyte (H_2SO_4 and $LiClO_4$) solutions. Since they demonstrated a good balance between ion storage capacity, optical modulation, and CE, they are recognized as the optical electrochromic features for electrochromic device applications. A higher CE was seen in the WO_3 that was annealed at 400°C with a lower OFR (2 SCCM) and a higher concentration of the H_2SO_4 electrolyte solution but

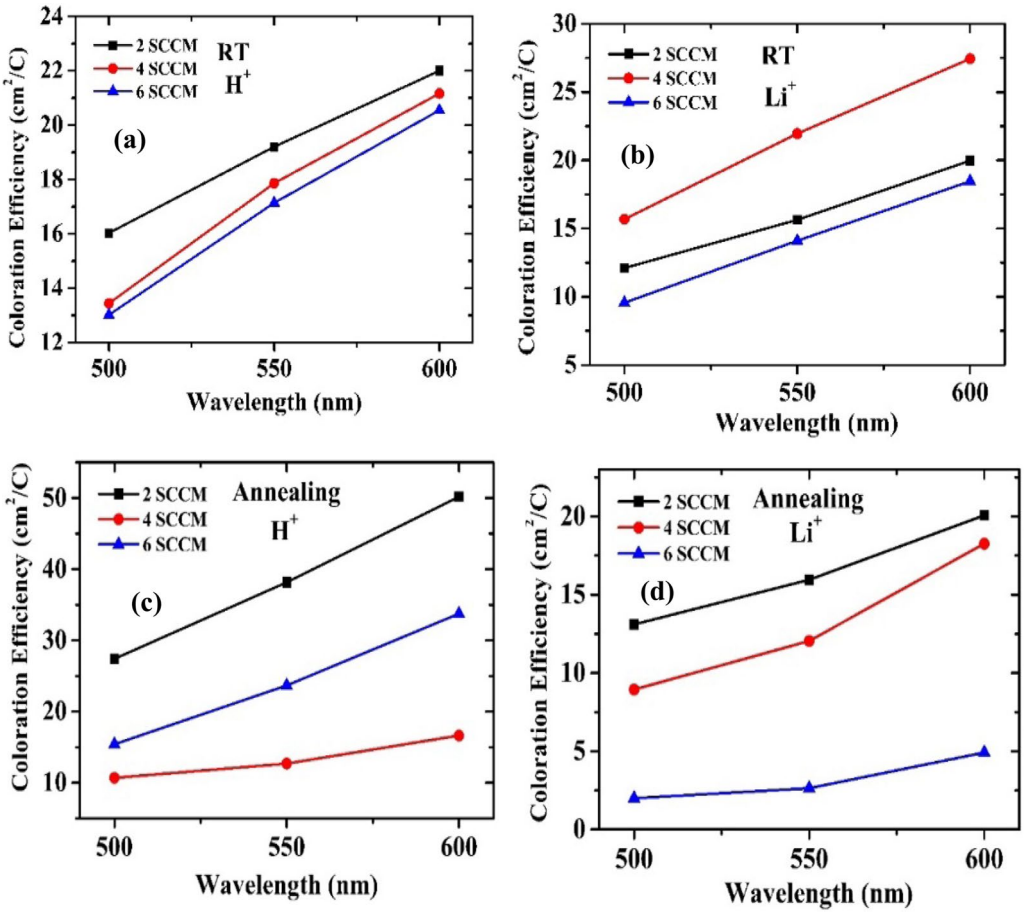

Fig. 14 Comparison of CE for H_2SO_4 (H^+) and $LiClO_4$ (Li^+) electrolytes: (a) and (b) RT WO_3 films and (c) and (d) annealed WO_3 films.

at the expense of switching properties, as shown by the prior data. The quick switching properties of crystalline WO_3 films, however, occur at the expense of low optical modulation.

Conclusion

This study revealed the effects of various OFRs (2, 4, and 6 SCCM) and annealing temperature on the structural, electrochromic, and optical characteristics of DC magnetron-sputtered WO_3 films. The WO_3 films are amorphous, according to XRD measurements; however, they exhibit crystalline characteristics at 400°C after annealing. SEM scans of WO_3 films revealed a uniform and smooth surface, which is a sign of its amorphous nature. The elimination of additional organic residues caused the WO_3 films to become denser with more evident cracks. Energy-dispersive x-ray spectroscopy (EDS) investigation demonstrated the absence of contaminants in the grown film and provided confirmation that W and O were present in the deposited film. We observed and carefully examined the effects of changing OFR and two different electrolyte solutions (H_2SO_4 and $LiClO_4$) on the electrochromic characteristics of the WO_3 and post-annealed WO_3 films. UV-visible spectrometry showed that the optical transmittance of higher OFRs and amorphous WO_3 samples was greater than that of lower OFRs and air-annealed samples. The amorphous WO_3 films in an electrolyte of H_2SO_4 at a 2 SCCM OFR is the highest DC of 1.007×10^{-7} cm^2/s in comparison to crystalline WO_3 films in an electrolyte of $LiClO_4$ at a 6 SCCM OFR. The optical modulation of amorphous WO_3 films in H_2SO_4 electrolyte solution is 86% at 6 SCCM OFR. In the CE results, crystalline WO_3 films in an electrolyte solution of H_2SO_4 performed better in an electrochemical cell than amorphous WO_3 films in an electrolyte solution of $LiClO_4$. Finally, we reach the conclusion that the electrolyte solution of H_2SO_4 contributes to improving the electrochromic properties of WO_3.

Acknowledgments The authors thank the Nitte Meenakshi Institute of Technology, Bengaluru, India, for providing facilities, and the work was supported by the Researchers Supporting Project number (RSPD2023R765), King Saud University, Riyadh, Saudi Arabia.

Data availability All data generated or analyzed during this study are included in this article and are available from the author.

Conflict of interest There is no conflict of interest to declare.

References

1. T. Brousse, D. Bélanger, K. Chiba, M. Egashira, F. Favier, J. Long, J.R. Miller, M. Morita, K. Naoi, P. Simon, and W. Sugimoto, Materials for electrochemical capacitors. *Springer Handbooks* (2017). https://doi.org/10.1007/978-3-662-46657-5_16.
2. R.S. Vemuri, M.H. Engelhard, and C.V. Ramana, Correlation between surface chemistry, density, and band gap in nanocrystalline WO_3 thin films. *ACS Appl. Mater. Interfaces* 4, 1371 (2012). https://doi.org/10.1021/am2016409.
3. C.G. Granqvist, Oxide electrochromics: an introduction to devices and materials. *Sol. Energy Mater. Sol. Cells* 99, 1 (2012). https://doi.org/10.1016/j.solmat.2011.08.021.
4. J. Gupta, H. Shaik, and K.N. Kumar, A review on the prominence of porosity in tungsten oxide thin films for electrochromism. *Ionics (Kiel)* 27, 2307 (2021). https://doi.org/10.1007/s11581-021-04035-8.
5. J. Gutpa, H. Shaik, K.N. Kumar, and S. Abdul, Materials Science in Semiconductor Processing PVD techniques proffering avenues for fabrication of porous tungsten oxide (WO_3) thin films : a review. *Mater. Sci. Semicond. Process.* 143, 106534 (2022). https://doi.org/10.1016/j.mssp.2022.106534.
6. M. Grätzel, Ultrafast colour displays. *Nature* 409, 575 (2001). https://doi.org/10.1038/35054655.
7. C.G. Granqvist, Electrochromics for smart windows: oxide-based thin films and devices. *Thin Solid Films* 564, 1 (2014). https://doi.org/10.1016/j.tsf.2014.02.002.
8. G.A. Niklasson and C.G. Granqvist, Electrochromics for smart windows :thin films of tungsten oxide and nickel oxide, and devices based on these. *J. Mater. Chem.* 17(2), 127 (2007). https://doi.org/10.1039/b612174h.
9. C.G. Granqvist, Electrochromic tungsten oxide films: review of progress 1993–1998. *Sol. Energy Mater. Sol. Cells* 60, 201 (2000). https://doi.org/10.1016/S0927-0248(99)00088-4.
10. H. Simchi, B.E. McCandless, T. Meng, and W.N. Shafarman, Structural, optical, and surface properties of WO_3 thin films for solar cells. *J. Alloy. Compd.* 617, 609 (2014). https://doi.org/10.1016/j.jallcom.2014.08.047.
11. Y.A.K. Reddy, B. Ajitha, A. Sreedhar, and E. Varrla, Enhanced UV photodetector performance in bi-layer TiO_2/WO_3 sputtered films. *Appl. Surf. Sci.* 494, 575 (2019). https://doi.org/10.1016/j.apsusc.2019.07.124.
12. A.V. Shchegolkov, S.H. Jang, A.V. Shchegolkov, Y.V. Rodionov, A.O. Sukhova, and M.S. Lipkin, A brief overview of electrochromic materials and related devices: a nanostructured materials perspective. *Nanomaterials* 11, 2376 (2021). https://doi.org/10.3390/nano11092376.
13. A.R. GV, H. Shaik, K.N. Kumar, V. Madhavi, H.D. Shetty, S.A. Sattar, M. Dhananjaya, B. Daruka Prasad, G.R. Kumar, and B.H. Doreswamy, Structural and electrochemical studies of WO_3 coated TiO_2 nanorod hybrid thin films for electrochromic applications. *Optik* 277, 170694 (2023). https://doi.org/10.1016/j.ijleo.2023.170694.
14. K. Naveen Kumar, H. Shaik, A. Pawar, L.N. Chandrashekar, S.A. Sattar, G. Nithya, R. Imran Jafri, V. Madhavi, J. Gupta, and G.V. Ashok Reddy, Effect of annealing and oxygen partial pressure on the RF sputtered WO_3 thin films for electrochromic applications. *Mater. Today: Proc.* 59, 339 (2022). https://doi.org/10.1016/j.matpr.2021.11.185.
15. K. Naveen Kumar, H. Shaik, L.N. Chandrashekar, P. Aishwarya, S. Abdul Sattar, G. Nithya, V. Madhavi, R. Imran Jafri, J. Gupta, and G.V. Ashok Reddy, On ion transport during the electrochemical reaction on plane and GLAD deposited WO_3 thin films. *Mater. Today Proc.* 59, 275 (2022). https://doi.org/10.1016/j.matpr.2021.11.113.
16. L. Geng, Gas sensitivity study of polypyrrole/WO_3 hybrid materials to H2S. *Synth. Met.* 160, 1708 (2010). https://doi.org/10.1016/j.synthmet.2010.06.005.
17. M. Trapatseli, D. Vernardou, P. Tzanetakis, and E. Spanakis, Field emission properties of low-temperature, hydrothermally grown tungsten oxide. *ACS Appl. Mater. Interfaces* 3, 2726 (2011). https://doi.org/10.1021/am200519w.
18. R. Mukherjee and P.P. Sahay, Improved electrochromic performance in sprayed WO_3 thin films upon Sb doping. *J. Alloy. Compd.* 660, 336 (2016). https://doi.org/10.1016/j.jallcom.2015.11.138.
19. N. Naseri, R. Azimirad, O. Akhavan, and A.Z. Moshfegh, Improved electrochromical properties of sol-gel WO_3 thin films by doping gold nanocrystals. *Thin Solid Films* 518, 2250 (2010). https://doi.org/10.1016/j.tsf.2009.08.001.
20. J. Thangala, S. Vaddiraju, R. Bogale, R. Thurman, T. Powers, B. Deb, and M.K. Sunkara, Large-scale, hot-filament-assisted synthesis of tungsten oxide and related transition metal oxide nanowires. *Small* 3, 890 (2007). https://doi.org/10.1002/smll.200600689.
21. J. Zhang, X.L. Wang, X.H. Xia, C.D. Gu, Z.J. Zhao, and J.P. Tu, Enhanced electrochromic performance of macroporous WO_3 films formed by anodic oxidation of DC-sputtered tungsten layers. *Electrochim. Acta* 55, 6953 (2010). https://doi.org/10.1016/j.electacta.2010.06.082.
22. K. Naveen Kumar, H. Shaik, Sathish, V. Madhavi, and S. Abdul Sattar, On the bonding and electrochemical performance of sputter deposited WO_3 thin films. *IOP Conf. Ser. Mater. Sci. Eng.* 872, 012147 (2020). https://doi.org/10.1088/1757-899X/872/1/012147.
23. K.N. Kumar, S.A. Sattar, G.V. Ashok Reddy, R.I. Jafri, R. Premkumar, M.R. Meera, A.A. Ahamed, M. Muthukrishnan, M. Dhananjaya, and A.M. Tighezza, Structural, optical, and electrochromic properties of RT and annealed sputtered tungsten trioxide (WO3) thin films for electrochromic applications by using GLAD technique. *J. Mater. Sci. Mater. Electron.* 34, 1934 (2023). https://doi.org/10.1007/s10854-023-11285-x.
24. K.N. Kumar, G. Nithya, H. Shaik, L.N. Chandrashekar, P. Aishwarya, and A.S. Pawar, Optical and electrochromic properties of DC magnetron sputter deposited tungsten oxide thin films at different electrolyte concentrations and vertex potentials for smart window applications. *J. Mater. Sci. Mater. Electron.* 34, 789 (2023). https://doi.org/10.1007/s10854-023-10180-9.
25. A.R. GV, K.N. Kumar, S. Abdul, H.D. Shetty, N. Guru, R.I. Jafri, C. Devaraja, B.C. Manjunatha, C.S. Kaliprasad, R. Premkumar, and S. Ansar, Physica B: condensed Matter Effect of post annealing on DC magnetron sputtered tungsten oxide (WO_3) thin films for smartwindow applications. *Phys. B Condens Matter* 664, 414996 (2023). https://doi.org/10.1016/j.physb.2023.414996.
26. K.N. Kumar, H. Shaik, J. Gupta, S. Abdul, I. Jafri, A. Pawar, V. Madhavi, A.R. GV, and G. Nithya, Sputter deposited tungsten oxide thin films and nanopillars: electrochromic perspective. *Mater. Chem. Phys.* 278, 125706 (2022). https://doi.org/10.1016/j.matchemphys.2022.125706.
27. K. Naveen Kumar, G. Nithya, H. Shaik, B. Hemanth, M. Chethana, K. Kishore, V. Madhavi, R.I. Jafri, S.A. Sattar, J. Gupta, and G.V. Ashok Reddy, Simulation and fabrication of tungsten oxide thin films for electrochromic applications. *Phys. B Condens Matter* 640, 413932 (2022). https://doi.org/10.1016/j.physb.2022.413932.
28. K.N. Kumar, S.A. Sattar, H. Shaik, A.R. GV, R.I. Jafri, M. Dhananjaya, A.S. Pawar, N.G. Prakash, R. Premkumar, S. Ansar,

L.N. Chandrashekar, and P. Aishwarya, Effect of partial pressure of oxygen, target current, and annealing on DC sputtered tungsten oxide (WO_3) thin films for electrochromic applications. *Solid State Ion* 399, 116275 (2023). https://doi.org/10.1016/j.ssi.2023.116275.

29. G.V. Ashok Reddy, H. Shaik, K. Naveen Kumar, R. Imran Jafri, S.A. Sattar, J. Gupta, and B.H. Doreswamy, Thickness dependent tungsten trioxide thin films deposited using DC magnetron sputtering for electrochromic applications. *Mater. Today Proc.* (2022). https://doi.org/10.1016/j.matpr.2022.11.134.
30. K. Naveen Kumar, H. Shaik, V. Madhavi, R. Imran Jafri, J. Gupta, G. Nithya, S.A. Sattar, and G.V. Ashok Reddy, Glancing angle sputter deposited tungsten trioxide (WO_3) thin films for electrochromic applications. *Appl. Phys. A Mater. Sci. Process.* 128, 1 (2022). https://doi.org/10.1007/s00339-022-06124-5.
31. G. Nithya, K.N. Kumar, R. Sai Yashwanth, W. Baig, S.V. Sai Ganesh, S. Hanvish Kumar, Simulation, deposition, and characterization of WO_3 and multilayered WO_3/Ag thin film structure for smart window applications, in: 2023 International Conference on Recent Advances in Science and Engineering Technology (ICRASET, IEEE, 2023), pp. 1–3. https://doi.org/10.1109/ICRASET59632.2023.10420072.
32. V. Madhavi, P. Kondaiah, H. Shaik, K.N. Kumar, T.S.S. Kumar Naik, G.M. Rao, and P.C. Ramamurthy, Fabrication of porous 1D WO_3 NRs and WO_3/$BiVO_4$ hetero junction photoanode for efficient photoelectrochemical water splitting. *Mater. Chem. Phys.* 274, 125095 (2021). https://doi.org/10.1016/j.matchemphys.2021.125095.
33. K.N. Kumar, G. Nithya, H. Shaik, L.N. Chandrashekar, P. Aishwarya, and A.S. Pawar, Optical and electrochromic properties of DC magnetron sputter deposited tungsten oxide thin films at different electrolyte concentrations and vertex potentials for smart window applications. *J. Mater. Sci. Mater. Electron.* 34, 789 (2023). https://doi.org/10.1007/s10854-023-10180-9.
34. J. Gupta, H. Shaik, K.N. Kumar, S.A. Sattar, and G.V.A. Reddy, Optimization of deposition rate for E-beam fabricated tungsten oxide thin films towards profound electrochromic applications. *Appl. Phys. A Mater. Sci. Process.* 128, 1 (2022). https://doi.org/10.1007/s00339-022-05609-7.
35. J. Gutpa, H. Shaik, K. Naveen Kumar, and S.A. Sattar, Optimization of GLAD angle for E-beam-fabricated Tungsten oxide (WO_3) thin films towards novel electrochromic behavior. *J. Electron. Mater.* (2022). https://doi.org/10.1007/s11664-022-10036-8.
36. J.Z. Ou, S. Balendhran, M.R. Field, D.G. McCulloch, A.S. Zoolfakar, R.A. Rani, S. Zhuiykov, A.P. O'Mullane, and K. Kalantar-Zadeh, The anodized crystalline WO_3 nanoporous network with enhanced electrochromic properties. *Nanoscale* 4, 5980 (2012). https://doi.org/10.1039/c2nr31203d.
37. J. Zhang, J.P. Tu, X.H. Xia, X.L. Wang, and C.D. Gu, Hydrothermally synthesized WO_3 nanowire arrays with highly improved electrochromic performance. *J. Mater. Chem.* 21, 5492 (2011). https://doi.org/10.1039/c0jm04361c.
38. A.R. GV, K. Naveen Kumar, H. Shaik, H.D. Shetty, R. Imran Jafri, S. Abdul Sattar, K. Kamath, and B.H. Doreswamy, Growth of cerium oxide nanorods by hydrothermal method and electrochromic properties of CeO_2/WO_3 hybrid thin films for smart window applications. *Mater. Today Proc.* (2022). https://doi.org/10.1016/j.matpr.2022.11.316.
39. G.V. Ashok Reddy, S.A. Sattar, K. Naveen Kumar, C.S. KaliPrasad, C. Devaraja, R. Imran Jafri, and B.H. Doreswamy, Effect of tungsten oxide thin films deposited on cerium oxide nano rods for electrochromic applications. *Opt. Mater.* 134, 113220 (2022). https://doi.org/10.1016/j.optmat.2022.113220.
40. A.R. GV, K.N. Kumar, H. Shaik, R.I. Jafri, R. Naik, and B.H. Doreswamy, Optical and electrochromic properties of CeO_2/WO_3 hybrid thin films prepared by hydrothermal and sputtering. *Int. J. Eng. Trends Technol.* 70, 1 (2022).
41. G.V. Ashok Reddy, K.N. Kumar, S.A. Sattar, N.G. Prakash, B. Daruka Prasad, M. Dhananjaya, G.R. Kumar, H.S. Yogananda, S.M. Hunagund, and S. Ansar, Structural, optical, and electrochromic properties of rare earth material (CeO_2)/transitional metal oxide (WO_3) thin film composite structure for electrochromic applications. *Ionics* (2023). https://doi.org/10.1007/s11581-023-05078-9.
42. G.F. Cai, J.P. Tu, D. Zhou, X.L. Wang, and C.D. Gu, Growth of vertically aligned hierarchical WO_3 nano-architecture arrays on transparent conducting substrates with outstanding electrochromic performance. *Sol. Energy Mater. Sol. Cells* 124, 103 (2014). https://doi.org/10.1016/j.solmat.2014.01.042.
43. V. Madhavi, P. Kondaiah, O.M. Hussain, and S. Uthanna, Structural, optical, and luminescence properties of reactive magnetron sputtered tungsten oxide thin films. *Int. Scholar. Res. Not.* 2012, 1 (2012). https://doi.org/10.5402/2012/801468.
44. S.H. Mohamed, H.A. Mohamed, and H.A. Abd El Ghani, Development of structural and optical properties of WOx films upon increasing oxygen partial pressure during reactive sputtering. *Phys. B* 406, 831 (2011). https://doi.org/10.1016/j.physb.2010.12.005.
45. S.H. Lee, H.M. Cheong, C.E. Tracy, A. Mascarenhas, D.K. Benson, and S.K. Deb, Raman spectroscopic studies of electrochromic a-WO_3. *Electrochim. Acta* 44, 3111 (1999). https://doi.org/10.1016/S0013-4686(99)00027-4.
46. J. Gabrusenoks, A. Veispals, A. Von Czarnowski, and K.H. Meiwes-Broer, Infrared and Raman spectroscopy of WO_3 and $CdWO_4$. *Electrochim. Acta* 46, 2229 (2001). https://doi.org/10.1016/S0013-4686(01)00364-4.
47. R. Chandra, A.K. Chawla, and P. Ayyub, Optical and structural properties of sputter-deposited nanocrystalline Cu_2O films: effect of sputtering gas. *J. Nanosci. Nanotechnol.* 6, 1119 (2006). https://doi.org/10.1166/jnn.2006.176.
48. A.K. Chawla, S. Singhal, H.O. Gupta, and R. Chandra, Effect of sputtering gas on structural and optical properties of nanocrystalline tungsten oxide films. *Thin Solid Films* 517, 1042 (2008). https://doi.org/10.1016/j.tsf.2008.06.068.
49. M.B. Babu and K.V. Madhuri, Synthesis and electrochromic properties of nanocrystalline WO_3 thin films. *Phys. B Condens. Matter* 584, 412068 (2020). https://doi.org/10.1016/j.physb.2020.412068.
50. C.K. Wang, D.R. Sahu, S.C. Wang, C.K. Lin, and J.L. Huang, Structural evolution and chemical bonds in electrochromic WO_3 films during electrochemical cycles. *J. Phys. D Appl. Phys.* 45, 225303 (2012). https://doi.org/10.1088/0022-3727/45/22/225303.
51. K.J. Patel, G.G. Bhatt, S.S. Patel, R.R. Desai, J.R. Ray, C.J. Panchal, P. Suryavanshi, V.A. Kheraj, and A.S. Opanasyuk, Thickness-dependent electrochromic properties of amorphous tungsten trioxide thin films. *J. Nano Electron. Phys.* 9, 03040 (2017). https://doi.org/10.21272/jnep.9(3).03040.
52. V. Madhavi, P. Kondaiah, O.M. Hussain, and S. Uthanna, Structural, optical and electrochromic properties of RF magnetron sputtered WO_3 thin films. *Phys. B* 454, 141 (2014). https://doi.org/10.1016/j.physb.2014.07.029.
53. C.S. Hsu, C.C. Chan, H.T. Huang, C.H. Peng, and W.C. Hsu, Electrochromic properties of nanocrystalline MoO_3 thin films. *Thin Solid Films* 516, 4839 (2008). https://doi.org/10.1016/j.tsf.2007.09.019.
54. B. Wen-Cheun Au, A. Tamang, D. Knipp, and K.Y. Chan, Post-annealing effect on the electrochromic properties of WO_3 films. *Opt. Mater.* 108, 110426 (2020). https://doi.org/10.1016/j.optmat.2020.110426.

55. X. Sun, Z. Liu, and H. Cao, Electrochromic properties of N-doped tungsten oxide thin films prepared by reactive DC-pulsed sputtering. *Thin Solid Films* 519, 3032 (2011). https://doi.org/10.1016/j.tsf.2010.12.017.